9.1 AIR-SEA INTERACTION EFFECTS ON MICROWAVE PROPAGATION OVER THE SEA DURING THE ROUGH EVAPORATION DUCT (RED) EXPERIMENT

Kenneth Anderson*, Paul Frederickson[1], Eric Terrill[2]
SPAWARSYSCEN, San Diego, California
[1]Naval Postgraduate School, Monterey, California
[2]Scripps Institution of Oceanography, La Jolla, California

1. INTRODUCTION

Microwave and electro-optical signal propagation over a wind-roughened sea is strongly dependent on signal interaction with the sea surface, the mean profiles of pressure (*P*), humidity (*Q*), temperature (*T*), wind (*U*) and their turbulent fluctuations (*p, q, t, u*). Yet, within the marine surface layer, these mechanisms are not sufficiently understood nor has satisfactory data been taken to validate propagation models, especially under conditions of high seas, high winds, and large surface gradients of *Q* and *T*. To address this deficiency, the Rough Evaporation Duct (RED) experiment was designed to provide first data for validation of meteorological, microwave, and electro-optical (EO) models in the marine surface layer for rough surface conditions including the effects of surface waves.

Over the ocean, "smooth-rough" surface similarity theory is often applied to construct profiles of *P, Q, T,* and *U* in the surface layer. In this context, the "rough" boundary layer is derived from empirical relations where ocean wave characteristics are neglected (*Fairall, et al., 1996).* For seas where wind speeds are less than 10-15 m/s and wave age near unity, there is excellent agreement for both meteorological and microwave propagation theory and measurements. However, recent evidence indicates that even small waves perturb *P, Q*, *T*, and *U* profiles throughout the surface layer (*cf Hristov, et al., 1998*). Indirect evidence of surface induced distortion of *P, Q*, and *T* profiles via modeling of the vertical microwave refractivity profile (*i.e.,* the evaporation duct) is indicated by analyses of previous microwave signal propagation experiments.

The RED experiment was conducted offshore of the Hawaiian Island of Oahu in late summer, mid-August to mid-September, of 2001. *R/P FLIP*, moored about 10 km off of the NE coast of Oahu, hosted the primary meteorological sensor suites and served as a terminus for the propagation links. There were eleven scientists and engineers aboard *R/P FLIP* who installed instruments measuring mean and turbulent meteorological quantities, sea wave heights, directions, and kinematics, upward and downward radiance, near surface-bubble generation, atmospheric particle size distributions, laser probing of the atmosphere, and sources for both microwave and electro-optic signals. In addition to *R/P FLIP*, two land sites were instrumented with microwave and EO receivers and meteorological sensors, two buoys were deployed, a small boat was instrumented, and two aircraft flew various tracks to sense both sea and atmospheric conditions. In all, more than 25 people from four countries, six universities, and four government agencies were directly involved with the RED experiment.

Analysis of the microwave data show a very good agreement between modeling, using the observed meteorological data to predict received signal levels, and the observed signal levels with means of the differences ranging from about 1 dB to 3 dB. However, with the low winds and wave heights observed during RED, the effects of surface waves are not readily isolated.

2. EXPERIMENTAL SETUP AND MODELING

Figure 1 illustrates the geometry of the RED experiment. *R/P FLIP* was three-point moored in about 300 m of water with its keel aligned into the Trade Winds that were, typically, from 080° at about 5 ms^{-1}. Its port boom, extending about 17 m from the hull in a northerly direction (see Figure 2) was fitted with a vertical mast that was instrumented with the sensors described in Table 1. Additional meteorological sensors were located on a 'flux-buoy' (*Frederickson, et al., 2003*) that was positioned mid-way between *R/P FLIP* and shore on the 10 km EO path (*Tsintikidis, et al., 2003*) and a 'mean-met' buoy positioned mid-way on the 27.7 km path. Two sets of three CW microwave transmitters,

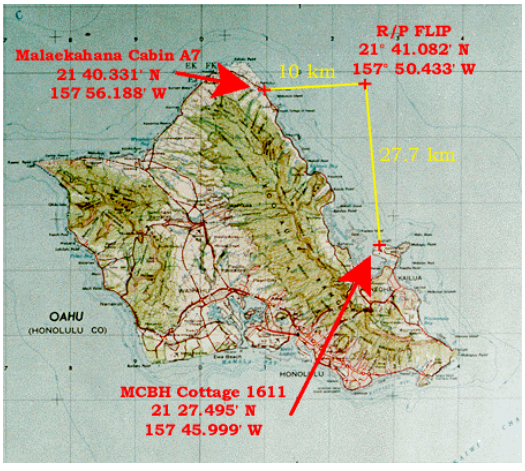

Figure 1. The geometry of the RED experiment.

* *Corresponding author address:* Kenneth D. Anderson, SPAWARSYSCEN, Code 2858, 53560 Hull St. San Diego, CA 92152; email: kenn@spawar.navy.mil

described in Table 2, were installed on the starboard side of *R/P FLIP*. The receiver site, located at the Marine Corps Base Hawaii, is shown in Figure 3 and details are provided in Table 2. From this site there was a clear unobstructed view to the transmitters located on *R/P FLIP*. Each transmitter was sampled sequentially in time at a 1 Hz rate for 256 seconds. The sequencing started at the hour and half-hour beginning with the high antenna then switching to the low antenna; the bands were sampled in order of Ku, X, then S. For the current work, the received signal levels were calibrated to propagation loss and then averaged into 5 minute intervals.

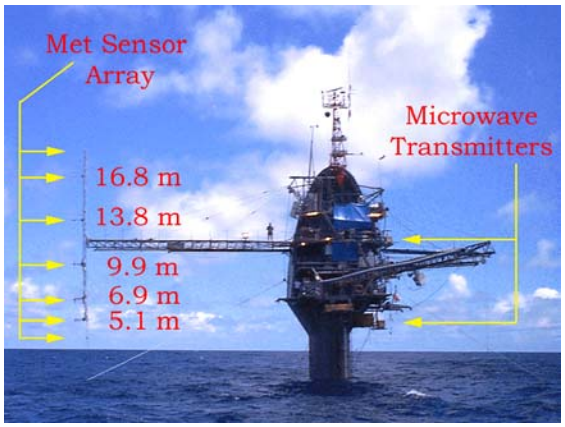

Figure 2. *R/P FLIP* as moored for RED.

Level	ASL (m)	Sensor
-1	0	S,H
0	3.1	G
1	5.1	C,L,D,H
2	6.9	C,L,D,H
3	9.9	C,L,D,H
4	13.8	C,K,D,H
5	16.8	G,D,H
6	19.8	A

A	Cup & Vane
C	Campbell CSAT3 Sonic
D	EdgeTech Dew Pointer
G	Gill Sonic
H	Hart Thermistor
K	Campbell Krypton Hygrometer
L	MM Lyman-Alpha Hygrometer
S	SIO Wavewire

Table 1. The met sensors installed by the University of California, Irvine (UCI) on the vertical array. (A) mean wind and direction, (C) & (G) 3D U, u, T, and t, (D) mean Q, (H) T, (K) & (L) Q and q, (S) sea surface elevation.

Propagation loss is defined as the ratio of the power transmitted by an antenna to the power received by another antenna but normalized to unity gain for both antennas. This definition includes the effects of antenna patterns but not the gain of those antennas, and is different from the quantity path loss. Since the antenna pattern in many cases can affect the loss observed or computed from models, propagation loss is a more accurate description. Free-space propagation loss, L_f is

$$L_f = \frac{P_r}{EIRP} = \left(\frac{\lambda}{4\pi R}\right)^2, \qquad (1)$$

Figure 3. The receiver antenna located at the Marine Corps Base Hawaii, Oahu, HI.

	S-band 3.0 GHz	X-Band 9.7 GHz	Ku-band 17.7 GHz
P_t (dBm)	30.0	30.0	33.0
G_t (dBi)	16.5	20.0	20.0
G_r (dBi)	26.0	37.0	42.0
G_{lna} (dB)	25.0	25.0	25.0
L_{max} (dB)	175.0	185.0	195.0
P_r (dBm)	-77.5	-73.0	-75.0
F_h (MHz)	3007.5	9824.5	17795.0
F_l (MHz)	2967.4	9624.0	17550.0
Z_h (m ASL)	12.6	12.6	12.6
Z_l (m ASL)	4.8	4.8	4.8
Z_r (m MSL)	4.5	4.5	4.5

Table 2. The microwave link design parameters for RED. The subscript h denotes the high-sited transmitters and the subscript l denotes the low-sited transmitters. L_{max} is the estimated propagation loss due to troposcatter (*Yeh, 1960*), which is the maximum loss expected for the link. The receiver, a HP 8566B Spectrum Analyzer, was operated with a 5 KHz bandwidth, yielding a noise floor approximately 20 dB below the design P_r.

where P_r is the received power in dBm, *EIRP* is the effective isotropic radiated power, which is the sum of P_t (transmitted power in dBm) and G_t (Gain of the transmitter antenna), λ is the wavelength, and R is the range between the transmitter and receiver. For the RED microwave links, P_r is given by

$$P_r = P_t + G_t - L_p - R \cdot m_a + G_t + G_{\ln a}, \qquad (2)$$

where L_p is the propagation loss, m_a is the molecular attenuation rate (dB/km), which, knowing the meteorology, is readily computed (*Liebe, 1985*) and G_{lna} is the gain of the low-noise amplifier.

Modeling of propagation loss is a two step process. First, mean values (5 minute averages) of sea temperature, T_s, with values of *T*, *Q*, and *U* measured at a reference height above the sea are processed using the Naval Postgraduate School (NPS) "bulk model" (*Frederickson, et al., 2003*) to estimate the vertical profile of radio refractive index, *n* (*Bean and Dutton, 1966*). Refractivity, *N*, is defined as $(n\text{-}1)10^6$ and modified refractivity, *M*, defined as $N+(z/a)10^6$, where *z* is the height above the surface and *a* is the earth's radius, is a conformal mapping from cylindrical coordinates into Cartesian coordinates, which simplifies evaluation of the wave equation. *N* is related to the observables as

$$N = 77.6\frac{P}{T} + \frac{3.73 \cdot 10^5 e}{T^2}, \qquad (3)$$

where *P* is the pressure (HPa), *e* is the water vapor pressure (HPa), and *T* is temperature (K) of the air parcel.

In the second step, the vertical *M* profile and a surface roughness parameter, σ, which is the rms "bump height" of the surface and is given by $0.0051\,U^2$ (*Phillips, 1966*), are processed by the Advanced Propagation Model (APM) to estimate propagation loss for each frequency and link geometry. APM (*Barrios, 2002*) uses the parabolic equation (PE) method (*Levy, 2000*) to approximate the 2D wave equation. While PE can handle range varying *M* profiles and surface conditions, only one *M* profile and one σ value were used at a time to represent the entire path. Although the PE formulation used in APM allows for complex *n* the molecular attenuation rate was computed from the averaged meteorological observables, scaled by the range, and added to the APM computed propagation loss.

3. OBSERVED AND MODELED PROPAGATION LOSS

Figure 4 illustrates the comparison of observed and modeled propagation loss for the high-sited and low-sited X-band links during RED. The reference lines labeled "free space" correspond to the propagation loss expected if the link paths were in free space, that is, a vacuum with no obstructions between the transmitters and receiver. The reference lines labeled "troposcatter" correspond to the propagation loss expected for the antennas sited as they were on the earth's surface but with atmospheric conditions of a well-mixed troposphere with a monotonic refractive gradient of 118 M/km. The observed signal levels (blue dots) are consistently near free-space for the high transmitter and nearly always exceed free-space levels for the low transmitter. The

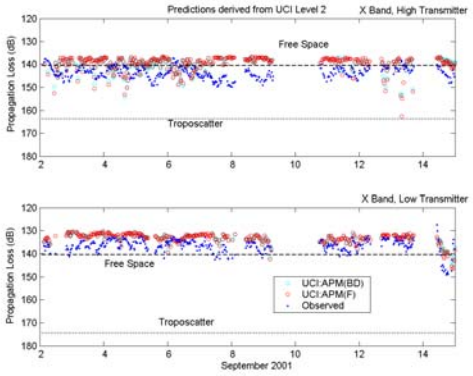

Figure 4. A comparison of observed to modeled propagation loss for the RED X-band microwave links. The meteorological data are from the UCI Level 2 sensor array with the cyan circles indicating use of the Businger-Dyer Phi functions and the red circles indicating use of the Friehe Phi functions.

mean and standard deviation of the difference between the observed and modeled (red and cyan circles) propagation loss is 0.8- and 3.4 dB for the high sited transmitter and 3.4- and 2.8 dB for the low sited transmitter. The modeled data for this example were derived using the meteorological data collected by UCI at level 2 on the vertical array. The NPS bulk model was modified to use both the standard Businger-Dyer profile functions of *T* and *Q* and a new form of the functions, suggested by C. Friehe (*Friehe, 2003*) that were derived from the UCI vertical array sensors during RED.

Tables 3 to 6 list the minimum, maximum, mean, and standard deviation of the difference between the observed and calculated propagation loss for all models, geometries, and frequencies. Considering the mean and standard deviation, all models are essentially equally good predictors.

4. CONCLUSIONS

Calculated results of the propagation model using meteorological inputs from either the UCI array or the NPS buoy in combination with either the Friehe or Businger-Dyer Phi function forms yield essentially the same standard deviation and mean. It is surprising to note that the Friehe form of the Phi functions (both H and Q) do not lead to better predictions of the propagation model compared to the Businger-Dyer form. Additional analysis is needed to determine if there is any systematic preference for using either the Friehe or Businger-Dyer forms.

Minimum Difference in Propagation Loss Comparisons

Frequency	S Band				X Band				Ku Band			
Tx Height	High		Low		High		Low		High		Low	
Phi Function	Std	Mod	Std	Mod	Std	Mod	Std	Mod	Std	Mod	Std	Mod
UCI 1	-4.8	-5.3	-2.9	-3.6	-13.7	-14.6	-13.5	-15.2	-19.1	-20.0	-22.0	-25.1
UCI 2	-3.8	-4.3	-2.2	-2.9	-13.1	-12.1	-10.5	-12.1	-20.0	-21.3	-27.3	-23.3
UCI 4	-4.0	-4.2	-1.8	-2.2	-20.8	-25.5	-5.7	-6.4	-14.1	-13.3	-37.8	-30.3
UCI 5	-3.0	-3.1	-0.9	-1.4	-15.9	-28.0	-4.2	-4.4	-18.3	-14.3	-36.2	-36.9
NPS	-4.7	-5.5	-5.0	-5.7	-14.5	-24.7	-6.9	-8.0	-23.0	-21.5	-22.7	-23.4
Average	-4.1	-4.5	-2.6	-3.2	-15.6	-21.0	-8.2	-9.2	-18.9	-18.1	-29.2	-27.8

Table 3. The minimum difference between the observed and calculated propagation loss (dB) for the three frequency bands (S is 3.0 GHz, X is 9.7 GHz, and Ku is 17.7 GHz) and the two transmitter heights (High is ~13 m asl and Low is ~5 m asl). The calculated propagation loss was computed using two Phi functions (Std is Businger-Dyer form and Mod is Friehe form) with six sources for the meteorological inputs (UCI x corresponds to the xth level of UCI's sensor array on *R/P FLIP* and NPS indicates the buoy located approximately 5 km west of *R/P FLIP*). The Average row is the mean minimum difference over the six sources. The cells shaded cyan are at least one dB less than the absolute value of the Average and indicate a better-than-average performance of the prediction model using the meteorological source.

Maximum Difference in Propagation Loss Comparisons

Frequency	S Band				X Band				Ku Band			
Tx Height	High		Low		High		Low		High		Low	
Phi Function	Std	Mod	Std	Mod	Std	Mod	Std	Mod	Std	Mod	Std	Mod
UCI 1	8.8	8.5	7.2	7.5	10.5	10.0	10.0	9.8	8.7	8.8	16.0	16.0
UCI 2	8.6	8.3	7.4	7.6	11.8	11.4	10.0	10.5	10.2	9.9	15.5	15.6
UCI 4	8.7	8.3	7.8	8.3	11.0	10.5	10.6	10.9	10.9	10.8	15.5	15.6
UCI 5	8.8	8.5	8.0	8.5	12.2	11.7	12.1	11.3	11.7	11.4	15.6	15.7
NPS	8.1	8.9	7.3	8.5	12.4	11.3	12.2	12.4	11.4	11.5	16.9	15.2
Average	8.6	8.5	7.5	8.1	11.6	11.0	11.0	11.0	10.6	10.5	15.9	15.6

Table 4. The maximum difference between the observed and calculated propagation loss (dB) presented in the same form as Table 3. All models are essentially equal predictors for S Band and Ku Band low antenna.

Mean Difference in Propagation Loss Comparisons

Frequency	S Band				X Band				Ku Band			
Tx Height	High		Low		High		Low		High		Low	
Phi Function	Std	Mod	Std	Mod	Std	Mod	Std	Mod	Std	Mod	Std	Mod
UCI 1	2.7	2.6	2.5	2.5	0.2	0.1	3.3	3.2	-2.4	-2.4	-0.5	-0.3
UCI 2	2.7	2.6	2.6	2.6	0.8	0.7	3.4	3.3	-1.9	-1.9	-1.3	-1.1
UCI 4	2.9	2.9	3.1	3.1	-0.3	-0.5	3.5	3.4	-1.4	-1.4	-1.1	-1.0
UCI 5	3.4	3.4	3.7	3.7	-1.4	-1.7	3.8	3.7	-1.1	-1.1	0.3	0.4
NPS	1.9	2.0	1.8	2.0	1.9	1.5	4.5	4.4	0.5	0.3	2.1	2.4
Average	2.7	2.7	2.7	2.8	0.9	0.9	3.7	3.6	1.5	1.4	1.1	1.0

Table 5. The mean difference between the observed and calculated propagation loss (dB) presented in the nearly the same form as Table 3. Here, the Average row is the mean of the absolute value of the mean difference and the parchment-colored cells are the best predictors. All models are essentially equal predictors considering the mean difference between the observed and calculated loss.

Standard Deviation of the Propagation Loss Comparisons

Frequency	S Band				X Band				Ku Band			
Tx Height	High		Low		High		Low		High		Low	
Phi Function	Std	Mod	Std	Mod	Std	Mod	Std	Mod	Std	Mod	Std	Mod
UCI 1	2.3	2.4	2.0	2.1	3.6	3.6	3.1	3.2	5.1	5.1	6.5	6.5
UCI 2	2.2	2.3	2.0	2.0	3.3	3.4	2.8	2.8	4.9	4.9	6.8	6.5
UCI 4	2.1	2.3	1.9	2.0	4.0	4.2	2.7	2.7	4.8	4.7	7.3	7.3
UCI 5	2.0	2.2	1.7	1.8	4.5	5.0	2.9	2.9	5.4	5.2	7.8	7.7
NPS	2.1	2.3	2.0	2.1	3.2	3.6	2.5	2.6	5.3	5.1	5.6	5.6
Average	2.1	2.3	1.9	2.0	3.7	4.0	2.8	2.8	5.1	5.0	6.8	6.7

Table 6. The standard deviation of the difference between the observed and calculated propagation loss (dB) presented in the same form as Table 5. All models are essentially equal predictors considering the standard deviation of the difference between observed and predicted.

5. REFERENCES

Barrios, A., 2002: APM Ver. 1.3.1. CSCI Documents, SPAWARSYSCEN Tech. Doc. 3145, Sep.

Bean, B. R., and E.J. Dutton, 1966: Radio Meteorology, NBS Monograph 92

Fairall, C.W., E.F. Bradley, D.P. Rogers, J.B. Edson, and G.S. Young, 1996: Bulk parameterization of air-sea fluxes for the Tropical Ocean-Global Atmosphere Coupled Ocean-Atmosphere Response Experiment, *J. Geophys. Res.*, 101, 3747-3764.

Frederickson, P., K. Davidson, K. Anderson, S. Doss-Hammel, and D. Tsintikidis, 2003: Air-sea interaction processes observed from buoy and propagation measurements during the RED experiment, 12th ISA, 9-13 Feb., Long Beach, CA., Paper 9.3

Friehe, C. and T. Hristov, 2003: Flux-profile relationships over the open ocean, 12th ISA, 9-13 Feb., Long Beach, CA., Paper 6.7.

Hristov, C. Friehe, and S. Miller, 1998: Wave-coherent fields in air flow over ocean waves: Identification of cooperative behavior buried in turbulence, *Phys. Rev. Let.*, **81**(2), 5245-5248.

Levy, M., 2000: Parabolic equation methods for electromagnetic propagation, Institution of Electrical Engineers, London, U.K.

Liebe, H., 1985: An updated model for millimeter wave propagation in moist air, *Rad. Sci.*, **20**(5), 1069-1089.

Phillips, O.M., 1966: The dynamics of the upper ocean, Cambridge Univ. Press, London, U.K.

Tsintikidis, D., S. Doss-Hammel, P. Frederickson, and K. Davidson, 2003: Infrared propagation in the marine atmospheric surface layer: Extinction and refraction, 12th ISA, 9-13 Feb., Long Beach, CA., Paper 9.8.

Yeh, L.P., 1960: Simple methods for designing troposcatter circuits, *IRE Trans. Comm. Syst.*, **CS-8**, 193-198.